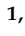




## Article

# Synthesis of AgCoCuFeNi High Entropy Alloy Nanoparticles by Hydrogen Reduction-Assisted Ultrasonic Spray Pyrolysis

Srecko Stopic <sup>1,\*</sup>, Ayadjenou Humphrey Hounsinou <sup>1</sup>, Tatjana Volkov Husovic <sup>2</sup>, Elif Emil-Kaya <sup>3</sup>  
and Bernd Friedrich <sup>1</sup>

<sup>1</sup> IME Process Metallurgy and Metal Recycling, RWTH Aachen University, 52056 Aachen, Germany; humphrey.hounsinou@rwth-aachen.de (A.H.H.); bfriedrich@ime-aachen.de (B.F.)

<sup>2</sup> Faculty of Technology and Metallurgy, University of Belgrade, Karnegijeva 4, 11000 Belgrade, Serbia; tatjana@tmf.bg.ac.rs

<sup>3</sup> Department of Materials Science and Engineering, Norwegian University of Science and Technology, 7034 Trondheim, Norway; elif.e.kaya@ntnu.no

\* Correspondence: sstopic@ime-aachen.de; Tel.: +49-241-80-95860

**Abstract:** Because of their high mixing entropies, multi-component alloys can exhibit enhanced catalytic activity compared to traditional catalysts in various chemical reactions, including hydrogenation, oxidation, and reduction processes. In this work, new AgCoCuFeNi high entropy alloy nanoparticles were synthesized by the hydrogen reduction-assisted ultrasonic spray pyrolysis method. The aim was to investigate the effects of processing parameters (reaction temperature, precursor solution concentration, and residence time) on the microstructure, composition, and crystallinity of the high entropy alloy nanoparticles. The characterization was performed with scanning electron microscope, energy-dispersive X-ray spectroscopy, and X-ray diffraction. The syntheses performed at 600, 700, 800, and 900 °C, resulted in smaller and smoother spherical particles with a near-equiatomic elemental composition as the temperature increased to 900 °C. With 0.25, 0.1, and 0.05 M precursor solutions, narrower size distribution and uniform AgCoCuFeNi nanoparticles were produced by reducing the solution concentration to 0.05 M. A near-equiatomic elemental composition was only obtained at 0.25 and 0.05 M. Increasing the residence time from 5.3 to 23.8 s resulted in an unclear particle microstructure. None of the five metal elements were formed in the large tubular reactor. X-ray diffraction revealed that various crystal phase structures were obtained in the synthesized AgCoCuFeNi particles.

**Keywords:** high entropy alloy; hydrogen reduction; ultrasonic spray pyrolysis; reaction temperature; precursor solution concentration; residence time



**Citation:** Stopic, S.; Hounsinou, A.H.; Husovic, T.V.; Emil-Kaya, E.; Friedrich, B. Synthesis of AgCoCuFeNi High Entropy Alloy Nanoparticles by Hydrogen Reduction-Assisted Ultrasonic Spray Pyrolysis. *ChemEngineering* **2024**, *8*, 63. <https://doi.org/10.3390/chemengineering8030063>

Academic Editors: Thomas Grütznier, Bernhard Seyfang and Antonio Monzon

Received: 7 November 2023

Revised: 8 June 2024

Accepted: 11 June 2024

Published: 18 June 2024



**Copyright:** © 2024 by the authors. Licensee MDPI, Basel, Switzerland. This article is an open access article distributed under the terms and conditions of the Creative Commons Attribution (CC BY) license (<https://creativecommons.org/licenses/by/4.0/>).

## 1. Introduction

Metals and their alloys have recently evolved from simple to complex component systems due to the increasing demand for materials with unique physical, chemical, or magnetic properties [1]. Usually, conventional alloys are based on one and rarely two principal elements [2] such as silver in sterling silver, iron in steel, and nickel in superalloys, with only smaller amounts of other elements. But this traditional strategy has become less successful due to the limited number of base elements in the periodic table [3]. Fortunately, a novel class of alloys based on multi-principal elements was independently introduced in 2004 by Yeh and his collaborators to reinforce the development of new materials. These complex metallic alloys, referred to as “high entropy alloys” (HEAs), are made by combining at least five well-mixed metal elements at near- equiatomic concentrations]. Because of their high mixing entropies, HEAs favor the formation of advanced materials with specific and diverse properties, including high thermal and chemical stability, excellent strength, outstanding corrosion and oxidation resistance, superconductivity, and magnetic prop-

erties [4,5]. Many of these properties cannot be achieved in conventional alloys, making HEAs a growing field of interest [6].

Moreover, HEAs will exhibit more interesting properties at the nanoscale compared to larger scales because of the very small size and shape of the particles. HEA nanoparticles (NPs) can be used in a variety of potential applications, particularly as high-performance catalysts [7]. The utilization of noble metal and noble metal-based oxide catalysts (such as Pt, RuO<sub>2</sub>, and IrO<sub>2</sub>), along with traditional alloy catalysts (like Fe-Pt, Pt-Ni, CuPdAu), in large-scale applications is hindered by their high costs, limited natural resources, and scarcity [8]. This creates a strong incentive to innovate and fabricate electrocatalysts that are cost-effective, exceptionally efficient, and easily accessible, surpassing the catalytic performance of noble metals and conventional alloys, hence the importance of HEAs in catalytic applications such as the hydrogen evolution reaction (HER), oxygen reduction reaction (ORR), oxygen evolution reaction (OER), CO<sub>2</sub> reduction reaction (CO<sub>2</sub>RR), and ammonia (NH<sub>3</sub>) decomposition [9]. In their study on the synthesis of Co CuFeNi particles by hydrogen reduction-assisted ultrasonic spray pyrolysis (USP-HR), Küçükelyas and his co-workers found that these particles exhibited high ferromagnetic behavior, making them promising materials for catalytic applications [10]. Also, silver (Ag) nanoparticles, due to their unique properties and high surface area, have often been used as catalysts in catalytic processes. The AgCoCuFeNi HEA NPs could therefore serve as highly effective catalysts.

A variety of methods such as laser scanning ablation [11], carbothermal shock [12], wet chemical reduction [13], moving bed pyrolysis [14], electrosynthesis [15], and ultrasonic spray pyrolysis [16] have been proposed for the synthesis of HEA NPs. Ultrasonic spray pyrolysis (USP) is often preferred due to the several distinct advantages it offers such as a low-cost, scalable, and continuous process; uniform particle size distribution; and finite and spherical grains [17–19]. In the USP technique, a metal precursor solution is used to produce an aerosol in an ultrasonic atomizer. The aerosol is subsequently transported into the heated reaction tube by a carrier gas, mainly a reducing agent. Within the tube, the aerosol droplets undergo evaporation, decomposition, and densification to form spherical particles. The desired particle size and morphology can be controlled by varying the precursor solution concentration, temperature, gas flow rate, and reactor dimensions [20,21].

The selection of an eco-friendly reducing agent is also another crucial measure to help lower the significant CO<sub>2</sub> emissions released from the metallurgical industry. In fact, the iron and steelmaking industry alone accounts for nearly 34% and 7% of industrial and global CO<sub>2</sub> emissions, respectively [22], motivating the replacement of carbon with hydrogen as the reducing agent for NPs [23].

So far, various HEA NPs, such as CoFeLaNiPt [15], NiCoCuFePt [24], and AgPdPt-CuNi [16], have been synthesized using diverse techniques. However, the combination of AgCoCuFeNi alloy and its particle synthesis via the hydrogen reduction-assisted ultrasonic spray pyrolysis (USP-HR) technique has not been explored. Therefore, this study aims to investigate the effects of processing parameters (reaction temperature, precursor solution concentration, and residence time) on the microstructure, composition, and crystallinity of the AgCoCuFeNi high entropy alloy nanoparticles. Specifically, the objectives consist of using scanning electron microscopy (SEM), energy dispersive X-ray spectroscopy (EDS), and X-ray diffraction (XRD) analyses to (1) study how the variation in furnace temperature influences the morphology, microstructure, composition, and crystallinity of AgCoCuFeNi NPs; (2) understand how the morphology, microstructure, composition, and crystallinity of AgCoCuFeNi NPs are modified through variation in precursor solution concentration; (3) and analyze the transition in morphology, microstructure, composition, and crystallinity of AgCoCuFeNi NPs due to the change in residence time.

## 2. Experimental Part

### 2.1. Material

An initial aqueous solution (0.5 mol/L, 1 L) was prepared by dissolving in deionized water an equimolar amount (0.1 mol) of five different reagents, silver nitrate (AgNO<sub>3</sub>),

cobalt nitrate hexahydrate  $[\text{Co}(\text{NO}_3)_2 \cdot 6\text{H}_2\text{O}]$ , copper nitrate trihydrate  $[\text{Cu}(\text{NO}_3)_2 \cdot 3\text{H}_2\text{O}]$ , iron nitrate nonahydrate  $[\text{Fe}(\text{NO}_3)_3 \cdot 9\text{H}_2\text{O}]$ , and nickel acetate tetrahydrate  $(\text{C}_4\text{H}_6\text{O}_4\text{Ni} \cdot 4\text{H}_2\text{O})$ . In contrast to the used metallic nitrate precursors, the subsequent decomposition of the basic nickel acetate at  $340^\circ\text{C}$  directly leads to the formation of either NiO or Ni, under treatment atmospheres of hydrogen. The autocatalytic NiO reduction to metallic nickel is the driving force to the reduction process of nickel acetate. During the major decomposition of the acetate group, a small amount of hydrogen is also evolved to the gas phase at about  $390^\circ\text{C}$ , which has a positive influence on the reduction process. On the other hand, CO production as a second reducing agent is expected mainly at  $350^\circ\text{C}$  and is interestingly the only product that can be obtained at  $900^\circ\text{C}$ , which accelerates the reduction process. All the chemicals were purchased from the Sigma-Aldrich company (St. Louis, MO, USA) and used as received without further purification because of their analytical grade ( $\geq 99\%$  pure). The solution was stirred for 1 h and diluted three times  $\{S_1(1:1), S_2(1:4), \text{ and } S_3(1:9)\}$  to obtain three precursor solutions with different concentrations, 0.25, 0.1, and 0.05 M, respectively.

## 2.2. Methods

The AgCoCuFeNi HEA NPs were synthesized by the hydrogen reduction-assisted ultrasonic spray pyrolysis (USP-HR) technique. A small tubular reactor was used to study the effect of temperature and concentration, while the small and large tubular reactors were used to investigate the influence of residence time on the particle microstructure, composition, and crystallinity. The USP-HR apparatus designed in our previous studies for the preparation of Fe-alloy NPs [25] was also used in this work for synthesizing AgCoCuFeNi NPs (Figure 1).

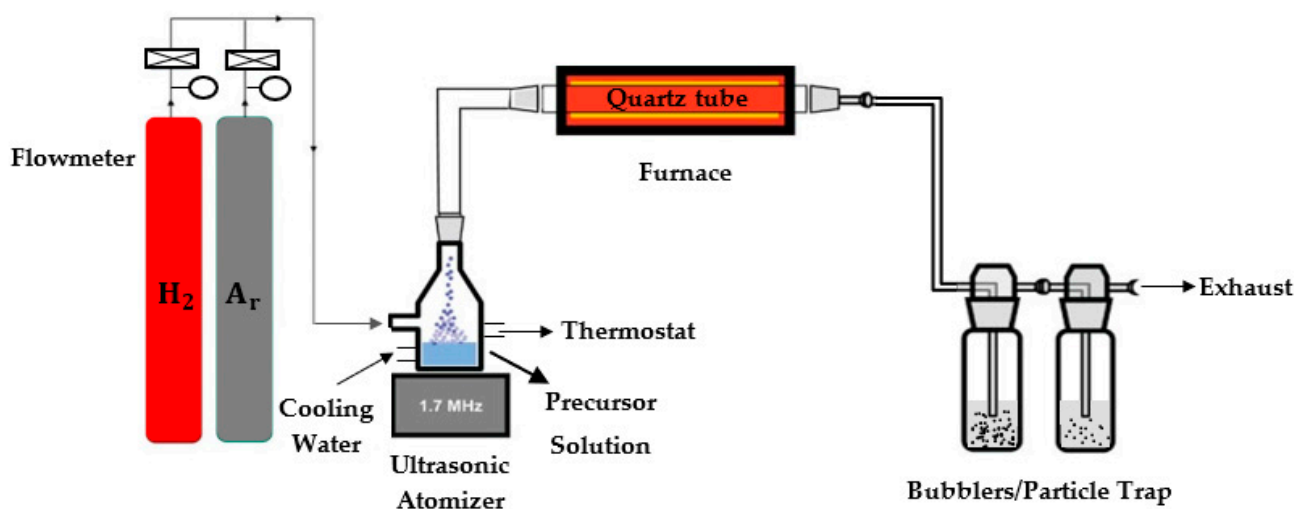


**Figure 1.** Schematic view of the USP-HR apparatus used for the AgCoCuFeNi high entropy nanoparticle synthesis.

### 2.2.1. Synthesis of AgCoCuFeNi NPs via the Small Tubular Reactor

The small tubular reactor involved a silica glass tube passing through two combined small furnaces (THERMOSTAR, Aachen, Germany). The experiment started by setting the furnace temperature. The HEA precursor solution was then nebulized at a frequency of 1.7 MHz into aerosol droplets. Water from the thermostat (JULABO, Seelbach, Germany) was used to cool the vessel to  $23^\circ\text{C}$ . The droplets were carried by a mixture of gases. Hydrogen gas was used as a reducing agent at a rate of 2 L/min while argon gas was used to transport the aerosol droplets into the reactor at a 1 L/min gas flow rate. Knowing the gas mixture flow rate (3 L/min) and the geometry of the tubular reactor heated by the

furnaces (l: 61 cm and d: 2.35 cm), the residence time of aerosol droplets inside the furnace was determined using Equation (1):

$$T = V_{\text{tube}}/q = \pi \cdot r^2 \cdot l/q \quad (1)$$

where  $q$  is the gas flow rate,  $r$  is the radius of the cylinder, and  $l$  is the length of the glass tube heated by the furnace. The calculated  $T$  was  $\sim 5.3$  s. Once the reduction process was finished, the resulting AgCoCuFeNi NPs were collected in the wash bottles connected to the reactor's outlet. The operating time for each experiment was 2 h. The details of the experimental parameters for the synthesis of AgCoCuFeNi NPs in the small tubular reactor are given in Table 1.

**Table 1.** Parameters used for the synthesis of AgCoCuFeNi NPs in the small tubular reactor.

Solution	No.	Concentration (mol/L)	Temperature (°C)
S <sub>1</sub>	1	0.25	600
	2	0.25	700
	3	0.25	800
	4	0.25	900
S <sub>2</sub>	5	0.1	600
	6	0.1	700
	7	0.1	800
	8	0.1	900
S <sub>3</sub>	9	0.05	600
	10	0.05	700
	11	0.05	800
	12	0.05	900

Due to the short residence time of aerosol droplets within the small reactor, the reaction time was also relatively short. However, the synthesis of spherical AgCoCuFeNi NPs typically requires a longer reaction time. For that purpose, a large furnace (CARBOLITE GERO, Neuhausen, Germany) with an alumina glass tube was used.

### 2.2.2. Synthesis of AgCoCuFeNi NPs via the Large Tubular Reactor

The precursor solution homogeneity is necessary for obtaining nanoparticles with uniform size and shape. Due to the unexpected formation of solid residues in the first and second precursor solutions (S<sub>1</sub> and S<sub>2</sub>) over time, only the third, more diluted solution S<sub>3</sub> with a concentration of 0.05 mol/L was used as the starting material in the large furnace setup. The AgCoCuFeNi nanoparticle synthesis method is the same in the Thermostar and Carbolite apparatus, except that the latter is automated (start and end time of the experiment, cooling system, and furnace temperature) with a large furnace. There are also differences in the settings. The large furnace heats up and cools down slower than the small one. The heating rate of the small furnace is about 900 °C/h while that of the large furnace is programmed at 300 °C/h. The large furnace should be left to cool to 500 °C before safely switching it off. This excessively prolongs the total duration of the experiment by approximately 3 h, which is more than the operating or reaction time (2 h). The residence time of droplets in the large tubular reactor was also calculated, knowing that the gas flow rate is the same (3 L/min), the furnace length (95 cm) equals the heating zone length, and the inner diameter of the alumina tube is 4 cm. Using Equation (1), the calculated residence time of aerosol droplets passing through the heating zone of the large tubular reactor was about 23.8 s. The experiments were performed on the precursor solution S<sub>3</sub> using the same parameters as in the small tubular reactor (Table 2).

**Table 2.** Parameters used for the synthesis of AgCoCuFeNi NPs in the large tubular reactor.

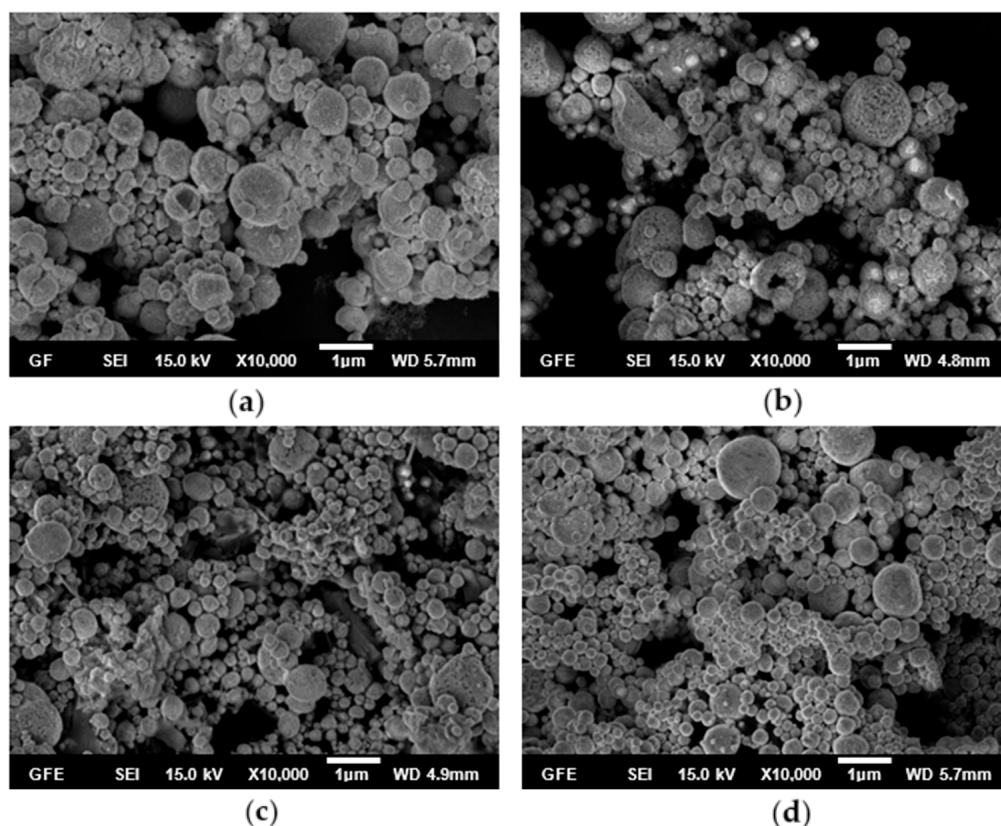
Solution	No.	Concentration (mol/L)	Temperature (°C)
S <sub>3</sub>	13	0.05	600
	14	0.05	700
	15	0.05	800
	16	0.05	900

After the synthesis process, sedimentation, and water removal, some of the particles were dried to obtain powders for X-ray diffraction (XRD) analysis. The particle suspensions were also sampled for scanning electron microscope (SEM) and energy dispersive X-ray spectroscopy (EDS) analyses. SEM images were taken using the Jeol JSM 7000F FEG-SEM (JEOL Ltd., Tokyo, Japan) and used to observe the surface morphology of particles formed at different reaction parameters. The particle size and size distribution were investigated from SEM images by ImagePro. EDS was carried out with a Si(Bi) X-ray detector connected to the SEM and a multi-channel analyzer to quantify the chemical composition of the particles. The crystal structure of the particles was determined by XRD (Philips-1700 X-ray diffractometer, Philips, Amsterdam, The Netherlands).

### 3. Results and Discussion

#### 3.1. Influence of Temperature on the AgCoCuFeNi HEA NPs

The effect of the reaction temperature on the particle size, morphology, and composition of AgCoCuFeNi nanoparticles was investigated while keeping the other parameters at constant values. SEM images of the particles synthesized in the small tubular reactor at 600, 700, 800, and 900 °C using 0.05 M precursor solution are shown in Figure 2.

**Figure 2.** SEM analysis of AgCoCuFeNi particles at (a) 600 °C, (b) 700 °C, (c) 800 °C, (d) 900 °C.

The SEM results show that almost all particles had a spherical morphology and appeared to be smoother on the surface with increasing temperature. Moreover, it was observed that the densification of small particles increased while the average particle size tended to decrease with increasing reaction temperature (Figures 2 and 3). The average particle sizes, calculated using ImagePro software V2, were 428, 382, 280, and 264 nm at 600, 700, 800, and 900 °C, respectively (Figure 3).

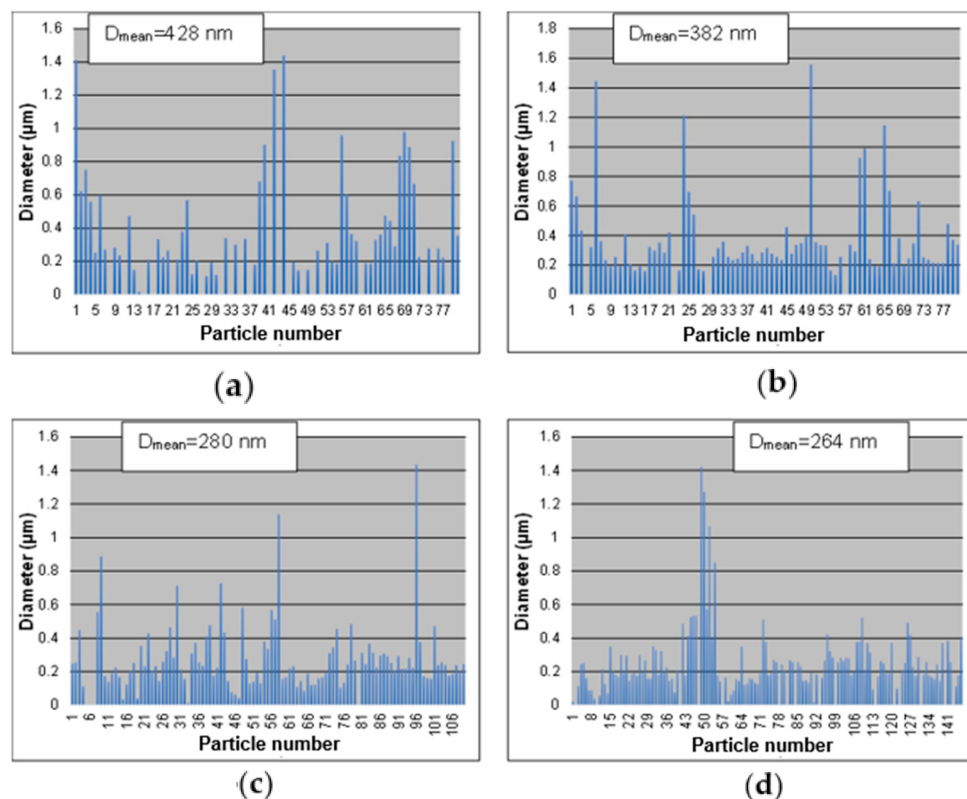


**Figure 3.** Mean diameters of AgCoCuFeNi particles at (a) 600 °C, (b) 700 °C, (c) 800 °C, (d) 900 °C.

The results of EDS analysis (Figure 4) of the AgCoCuFeNi HEA particles synthesized at different reaction temperatures, 600, 700, 800, and 900 °C, are given in Table 3. The results indicate that the elements making up the composition were present in close amounts at all reaction temperatures, suggesting that the AgCoCuFeNi HEA NPs were successfully formed using the USP-HR approach. When the temperature reached 900 °C, four of the metal elements (Ag, Co, Fe, and Ni) in the synthesized nanoparticles appeared to be in very similar proportions and their atomic percentages increased to 15.25% for Ag, 15.68% for Co, 15.05% for Fe, and 15.44% for Ni, while the percentage of Cu remained relatively large at all temperatures and increased to 21.2% at 900 °C. Because of the short residence time in the small furnace at higher temperatures, the reduction efficiency is different for the studied metals. This led to one difference in its chemical composition in the metallic alloy. As shown in Table 3, the oxygen content in the particles decreased from 28.33 to 16.99% with an increase in temperature from 600 °C to 900 °C, as proven in the work of Simić et al. [16]. Protecting the formed fine particles from oxidation poses a significant challenge. Additionally, an incomplete reduction in the precursor contributes to the presence of oxygen in the metallic alloy powder at different temperatures.

Small peaks of aluminum (Al), chlorine (Cl), and silicon (Si) were also detected in the EDS spectra. Al was used as the background material for EDS analysis. We believe that Si came from the use of the silica glass tube. During the USP-HR method for producing nanoparticles, it is possible that through heating the silica tube by the furnaces, small traces of silicon decomposed and infiltrated the particles. It is also possible that the water used

during precursor solution and sample preparation was not properly deionized. As a result, it may have contained impurities such as silicon and chlorine.

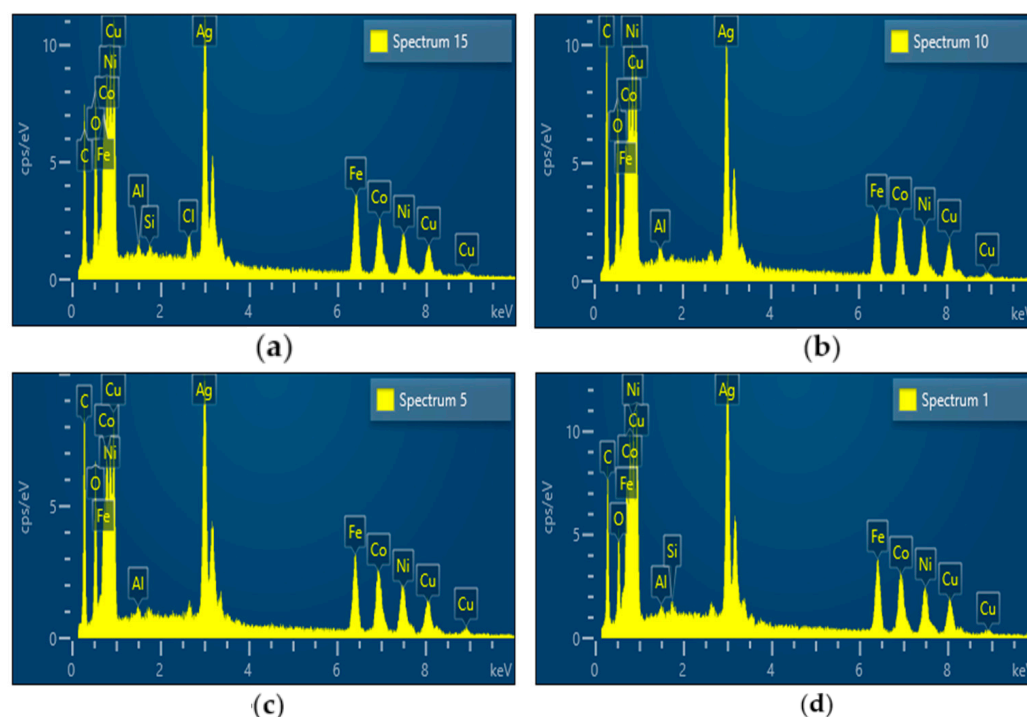


**Figure 4.** EDS spectra for AgCoCuFeNi particles at (a) 600 °C, (b) 700 °C, (c) 800 °C, (d) 900 °C.

**Table 3.** EDS results of AgCoCuFeNi NPs produced at different temperatures.

Temperature (°C)	Element (at.%)							
	Ag	Co	Cu	Fe	Ni	O	Al	Cl
600	13.06	11.77	19.55	14.35	12.09	28.33	–	0.91
700	11.77	14.04	18.09	11.79	15.17	28.24	0.78	0
800	12.96	14.79	17.57	13.85	14.66	25.53	0.60	0
900	15.25	15.68	21.2	15.05	15.44	16.69	0.66	0

Figure 5 illustrates the XRD patterns of the AgCoCuFeNi HEA NPs produced through hydrogen reduction-assisted ultrasonic spray pyrolysis. The XRD analysis revealed various phases, with two of them being identified as FCC phases [26]. The FCC phase with a high Ag content is labeled as Ag-rich FCC. Ag has a higher atomic mass compared to Co, Cu, Fe, and Ni, and Ag may not mix with other elements in the same FCC structure. The other FCC phase, designated as FCC-2, includes Fe, Co, Cu, and Ni, as their primary diffraction peaks overlap, and their atomic masses are closely situated to each other and FCC-2 is consistent with the lattice of Co/Ni. The small amount of Fe and Cu present on the surface is oxidized after the synthesis process, since the HEA powders are fine and have high surface area. We also noticed that with an applied magnetic field (e.g., magnet), all the AgCoCuFeNi nanopowder samples showed a magnetic behavior (Figure 6), mainly due to the presence of ferromagnetic materials (Fe, Ni, and Co) in the composition. Yet, specific characterization tools like a magnetic particle analyzer (MPA) are required to quantify or study the degree to which a sample exhibits magnetic properties compared to the others.

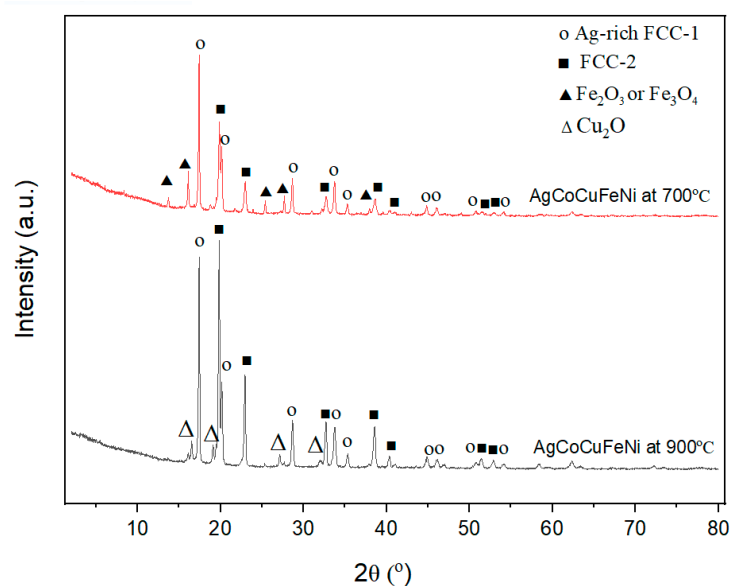


**Figure 5.** XRD patterns of AgCoCuFeNi particles.

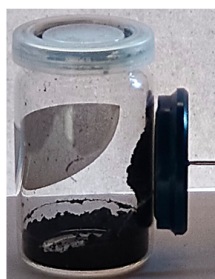


**Figure 6.** AgCoCuFeNi samples with magnetic properties.

### 3.2. Influence of Concentration on the AgCoCuFeNi HEA NPs

Here, the effects of the precursor solution concentration, ranging from 0.25, 0.1 to 0.05 M, on the particle size, morphology, and composition were investigated at 900 °C. SEM images of the AgCoCuFeNi particles are given in Figure 7. Particles prepared in all concentrations had a spherical morphology but became smoother on the surface with decreasing solution concentration. The AgCoCuFeNi particles exhibited a decreasing trend as the corresponding solution concentration decreased from 0.25 or 0.1 to 0.05 M but showed an increasing trend when the concentration was reduced from 0.25 to 0.1 M (Figure 8).

The average particle sizes for the synthesized AgCoCuFeNi particles using 0.25, 0.1, and 0.05 M solutions were 294, 641, and 264 nm, respectively. Moreover, it was observed that a narrower size distribution was obtained at 0.05 M and the size uniformity of the particles increased by reducing the solution concentration to 0.05 M (Figure 8).

EDS analysis indicates that AgCoCuFeNi particles produced from both precursor concentrations, 0.25 and 0.05 M, contained the five metal elements (Ag, Co, Cu, Fe, and Ni) in closer proportions than AgCoCuFeNi particles synthesized at 0.1 M. In particular, the atomic percentage of the Cu element remained relatively high at 0.25 and 0.05 M but was low at 0.1 M compared to the other metal elements present in the nanoparticles. In addition, the oxygen content decreased with decreasing precursor concentration (Table 4).



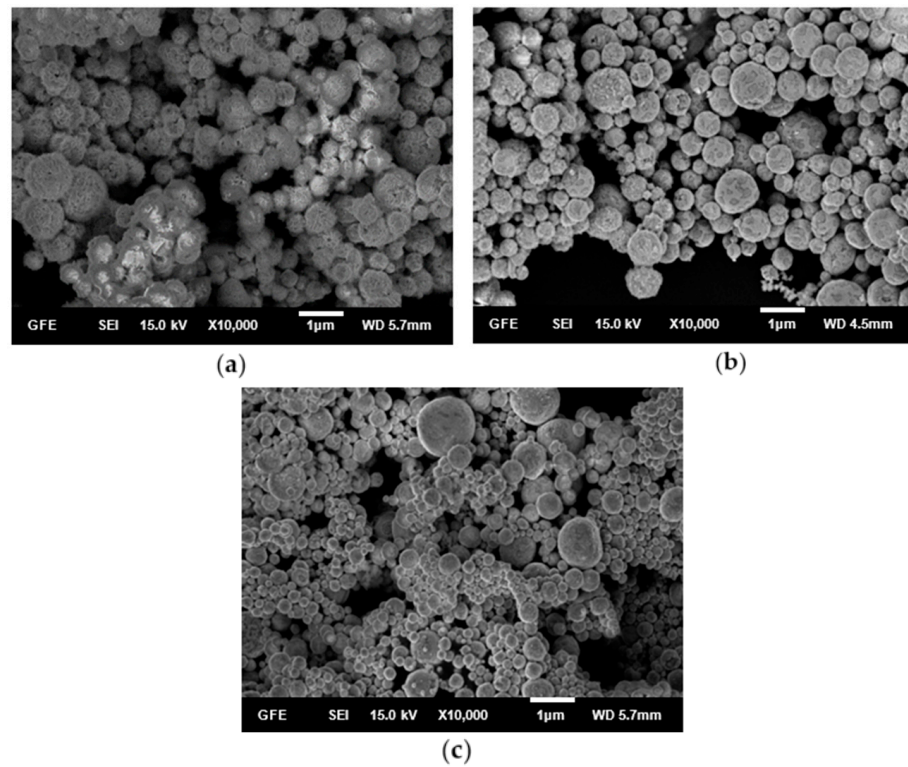


**Figure 7.** SEM analysis of AgCoCuFeNi particles at (a) 0.25 mol/L, (b) 0.1 mol/L, (c) 0.05 mol/L.

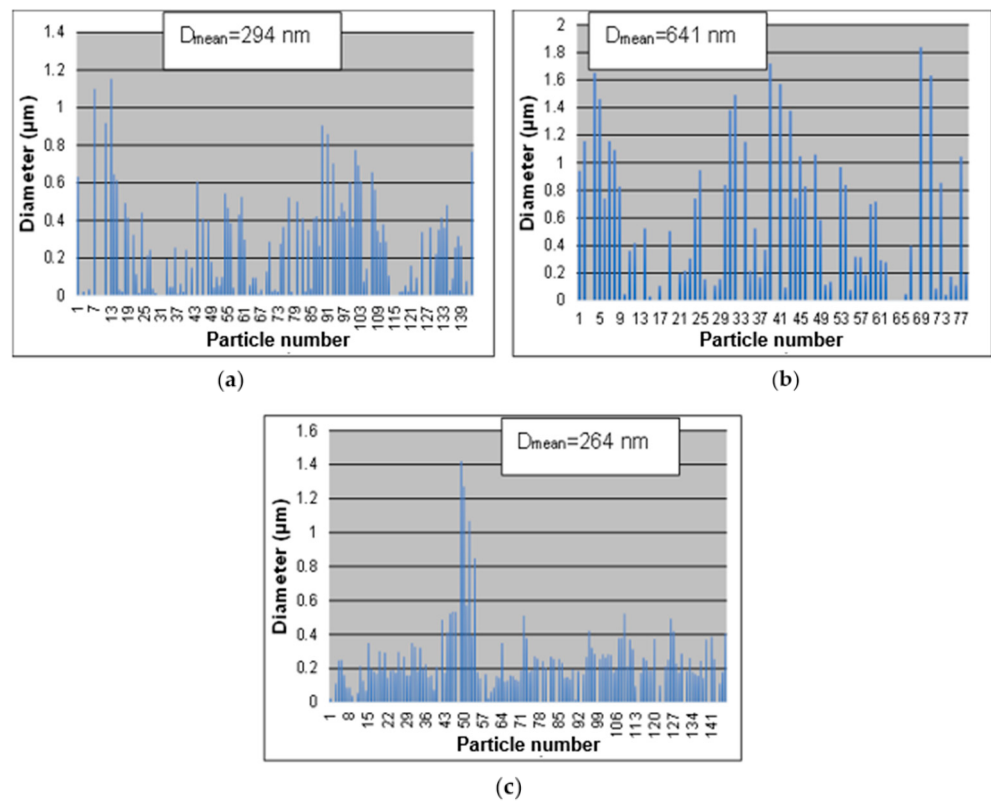


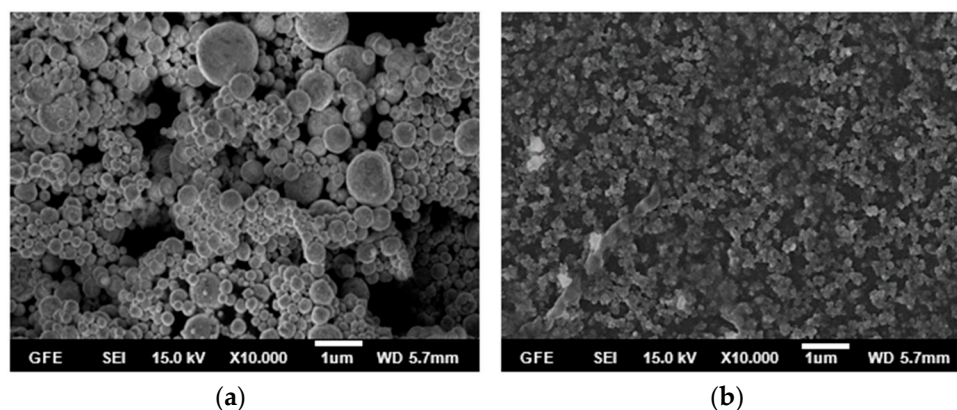
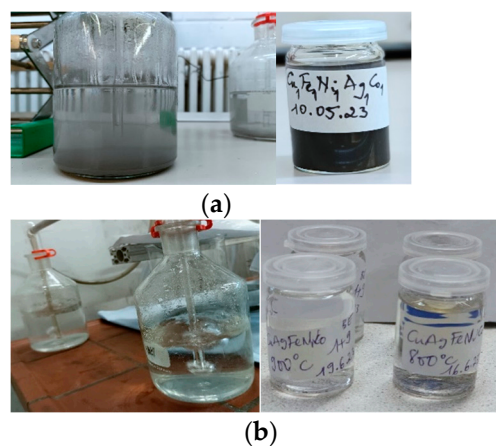
**Figure 8.** Mean diameters of AgCoCuFeNi particles at (a) 0.25, (b) 0.1, (c) 0.05 mol/L.

**Table 4.** EDS results of AgCoCuFeNi NPs produced at different concentrations at 900 °C.

Concentration (mol/L)	Element (at.%)						
	Ag	Co	Cu	Fe	Ni	O	Al
0.25	13.44	11.77	15.65	13.56	13.59	31.96	0
0.1	10.24	13.65	9.89	19.60	12.28	33.77	0.54
0.05	15.25	15.68	21.2	15.05	15.44	16.69	0.66

### 3.3. Influence of Residence Time

The effects of the residence time on the particle size, morphology, and composition of AgCoCuFeNi nanoparticles were also investigated using the 0.05 M precursor solution at 900 °C in the small and large tubular reactor. Spherical particles with smooth surfaces were obtained only from the small reactor with a short residence time of 5.3 s (Figure 9a). When the residence time was increased to 23.8 s using the large furnace, particles with an unclear structure but approximately spherical shape with rough surfaces were formed (Figure 9b). Indeed, the amount of AgCoCuFeNi particles obtained at the end of the USP-HR process in the wash bottles of the large furnace was very low compared to that of the small furnace (Figure 10). This made SEM analysis of the particles synthesized in the high-temperature setup more difficult.

**Figure 9.** SEM analysis of AgCoCuFeNi particles with residence time of (a) 5.3 s, (b) 23.8 s.**Figure 10.** AgCoCuFeNi particles synthesized with residence time of (a) 5.3 s, (b) 23.8 s.

The EDS spectrum of the particles synthesized with the residence time of 23.8 s clearly shows that none of the five metal elements constituting the AgCoCuFeNi HEA nanoparticles were formed (Figure 11).

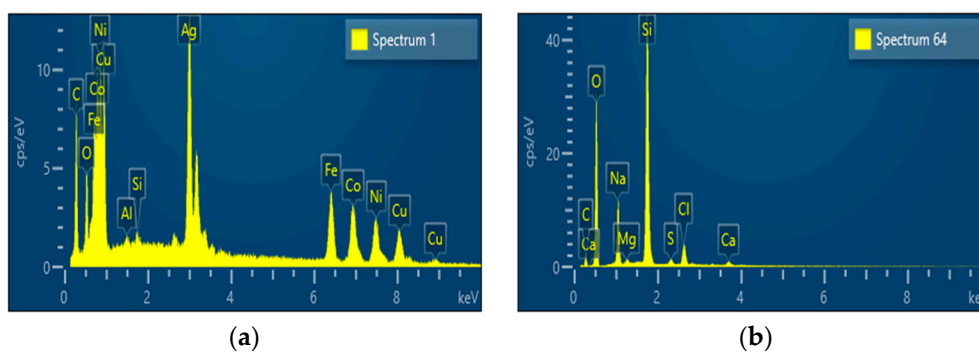


**Figure 11.** EDS spectra for AgCoCuFeNi particles with residence time of (a) 5.3 s, (b) 23.8 s.

We believe that more reaction or operating time is needed to obtain the desired nanoparticles since the residence time of aerosol droplets inside the large tubular reactor is approximately 4 times higher than that of the small tubular reactor. We also believe that the replacement of the alumina glass tube or the increase in the gas flow rate or in the ultrasonic frequency are essential parameters to be considered. The influence of the increased temperature on the residence time is not considered, but it is expected that an increased temperature leads to a decreased residence time. The pyrolysis time, and especially an increased residence time, increases the crystallinity of the prepared particles considerably as confirmed by Ardekani [27]. Therefore, an improvement in experimental setup can be performed via an increase in the reaction volume, increasing the radius and the length of the reaction tube.

In a system with a different precursor solution, a critical parameter in the preparation of fine and solid spherical particles is that the precipitated salts should not be deformed or melted during heating, since this issue results in the formation of shells of low permeability. Therefore, the chosen reaction temperatures are smaller than 1000 °C and its smelting points. As a result, the obtained solvent is trapped within the core of drying droplets leading to a higher pressure, since the solvent is not able to evaporate easily from the shell. Thus, the cracks formed on the shells produce secondary droplets and the broken shells lead to the formation of irregular-shaped particles, as shown at Figures 7 and 9. The salt solubility is not required to be high in order to form uniform and solid particles, but solution saturation should be avoided in order to prevent mass loss during an atomization process.

Finally, in the USP method, the spherical shape of the obtained particles results from the spherical droplets of the dissolved metallic salts in water. It is seen in the SEM images in Figures 7 and 9 that spherical particles as the daughter products are manifested from spherical liquid droplets as the mother droplets. The coalescence of the aerosol droplets through their transport using carrier and reduction gases such as hydrogen leads to an increased particle size and an agglomeration of particles. Therefore, the droplet-per-droplet transformation model cannot be applied in this system. The crystallite size increases as the calcination temperature increases in the used furnace.

#### 4. Conclusions

In the USP method, it is expected that the spherical shape of the obtained particles results from the spherical droplets of the mixture of precursor salts dissolved in water. It is evident that different shapes of particles in the SEM figures confirm the high influence of the transport phenomena and the coalescence of aerosol droplets. The collision of droplets leads to different particle sizes. Spherical equiatomic AgCoCuFeNi high entropy alloy nanoparticles were successfully produced via hydrogen reduction-assisted ultrasonic spray pyrolysis (USP-HR) at temperatures below the melting point of each alloying metal. This study focused on investigating the influence of reaction temperature, precursor solution concentration, and residence time on the particle size, morphology, composition, and

crystallinity of AgCoCuFeNi nanoparticles using SEM, EDS, and XRD characterization tools. The results are given below:

- The synthesis performed in the small tubular reactor at 600, 700, 800, and 900 °C starting from a 0.05 M precursor mixture of the five metal salts revealed that increasing the reaction temperature led to smaller and smoother spherical particles. The average particle size decreased from 428 to 264 nm with an increase in temperature from 600 to 900 °C. Four of the metal elements (Ag, Co, Cu, Fe, and Ni) making up the AgCoCuFeNi composition were present in very close proportions when the temperature reached 900 °C, while the at.% of Cu remained relatively large. The oxygen concentration in the synthesized particles decreased with increasing reaction temperature.
- The synthesis performed in the small tubular reactor with 0.25, 0.1, and 0.05 M precursor solutions at 900 °C resulted in a narrower size distribution and uniformity of the AgCoCuFeNi NPs by reducing the solution concentration to 0.05 M. The average particle sizes using 0.25, 0.1, and 0.05 M solutions were 294, 641, and 264 nm, respectively. The five metal elements appeared to be in closer proportions at 0.25 and 0.05 M than at 0.1 M concentrations. The atomic percentage of oxygen decreased with decreasing precursor solution concentrations.
- The synthesis performed in both the small and large tubular reactors with 0.05 M precursor solution at 900 °C revealed a decrease in the precision of the AgCoCuFeNi particle microstructure and composition as the residence time increased from 5.3 s (small setup) to 23.8 s (the large setup). None of the five metal elements were formed in the large tubular reactor.

AgCoCuFeNi nanoparticles, being a high entropy alloy with a complex composition, could exhibit enhanced catalytic activity compared to traditional catalysts in various chemical reactions (e.g., hydrogenation, oxidation, and reduction processes) and be used as electrode materials to potentially improve battery (e.g., lithium-ion batteries) performance and cycle life. The outcomes of this study provide valuable insights into optimizing the synthesis of AgCoCuFeNi nanoparticles. However, further research and development are needed to fully explore and validate the practical utility of AgCoCuFeNi nanoparticles in these fields and beyond.

In order to enable the continuous production of HEA using ultrasonic spray pyrolysis synthesis, a scale up of the studied process should be performed in five different horizontal lines with a continuous injection of solution. An improvement in collection efficiency should be performed using an electrostatic atomizer in contrast to the two bottles with water that were used.

**Author Contributions:** Conceptualization, A.H.H. and S.S.; methodology, S.S.; software, E.E.-K.; validation, A.H.H. and E.E.-K.; formal analysis, T.V.H.; investigation, A.H.H.; resources, S.S.; data curation, A.H.H.; writing—original draft preparation, A.H.H. and S.S.; writing—review and editing, S.S., visualization, E.E.-K.; supervision, S.S.; project administration, S.S.; funding acquisition, B.F. All authors have read and agreed to the published version of the manuscript.

**Funding:** This research was funded by the Federal Ministry of Education and Research, grant number 03SF0626C. The APC was funded by MDPI, Basel, Switzerland.

**Data Availability Statement:** No. But in future you can find our data on: IME Process Metallurgy and Metal Recycling ([www.rwth-aachen.de](http://www.rwth-aachen.de)).

**Conflicts of Interest:** The authors declare no conflicts of interest.

## References

1. Zhang, Y.; Zuo, T.T.; Tang, Z.; Gao, M.C.; Dahmen, K.A.; Liaw, P.K.; Lu, Z.P. Microstructures and properties of high-entropy alloys. *Prog. Mater. Sci.* **2014**, *61*, 1–93. [[CrossRef](#)]
2. Yeh, J.-W.; Chen, S.K.; Lin, S.-J.; Gan, J.-Y.; Chin, T.-S.; Shun, T.-T.; Tsau, C.-H.; Chang, S.-Y. Nanostructured High-Entropy Alloys with Multiple Principal Elements: Novel Alloy Design Concepts and Outcomes. *Adv. Eng. Mater.* **2004**, *6*, 299–303. [[CrossRef](#)]
3. Babić, E.; Drobac, Đ.; Figueroa, I.A.; Laurent-Brocq, M.; Marohnić, Ž.; Mikšić Trontl, V.; Pajić, D.; Perrière, L.; Pervan, P.; Remenyi, G.; et al. Transition from High-Entropy to Conventional Alloys: Which Are Better? *Materials* **2021**, *14*, 5824. [[CrossRef](#)] [[PubMed](#)]

4. Zhang, Y.; Zuo, T.; Cheng, Y.; Liaw, P.K. High-entropy Alloys with High Saturation Magnetization, Electrical Resistivity and Malleability. *Sci. Rep.* **2013**, *3*, 1455. [[CrossRef](#)] [[PubMed](#)]
5. Zou, Y.; Wheeler, J.M.; Ma, H.; Okle, P.; Spolenak, R. Nanocrystalline High-Entropy Alloys: A New Paradigm in High-Temperature Strength and Stability. *Nano Lett.* **2017**, *17*, 1569–1574. [[CrossRef](#)] [[PubMed](#)]
6. Miracle, D.B.; Senkov, O.N. A critical review of high entropy alloys and related concepts. *Acta Mater.* **2017**, *122*, 448–511. [[CrossRef](#)]
7. Katiyar, N.K.; Biswas, K.; Yeh, J.-W.; Sharma, S.; Tiwary, C.S. A perspective on the catalysis using the high entropy alloys. *Nano Energy* **2021**, *88*, 106261. [[CrossRef](#)]
8. Kim, J.; Shih, P.; Qin, Y.; Al-Bardan, Z.; Sun, C.; Yang, H. A Porous Pyrochlore  $Y_2[Ru_{1.6}Y_{0.4}]O_{7-\delta}$  Electrocatalyst for Enhanced Performance towards the Oxygen Evolution Reaction in Acidic Media. *Angew. Chem. Int. Ed.* **2018**, *57*, 13877–13881. [[CrossRef](#)] [[PubMed](#)]
9. Modupeola, D.; Popoola, P. High entropy nanomaterials for energy storage and catalysis applications. *Front. Energy Res.* **2023**, *11*, 1149446. [[CrossRef](#)]
10. Küçükelyas, B.; Safaltın, Ş.; Sam, E.D.; Gurmen, S. Synthesis, structural and magnetic characterization of spherical high entropy alloy CoCuFeNi particles by hydrogen reduction assisted ultrasonic spray pyrolysis. *Int. J. Mater. Res.* **2022**, *113*, 306–315. [[CrossRef](#)]
11. Wang, B.; Wang, C.; Yu, X.; Cao, Y.; Gao, L.; Wu, C.; Yao, Y.; Lin, Z.; Zou, Z. General synthesis of high-entropy alloy and ceramic nanoparticles in nanoseconds. *Nat. Synth.* **2022**, *1*, 138–146. [[CrossRef](#)]
12. Yao, Y.; Huang, Z.; Xie, P.; Lacey, S.D.; Jacob, R.J.; Xie, H.; Chen, F.; Nie, A.; Pu, T.; Rehwoldt, M.; et al. Carbothermal shock synthesis of high-entropy-alloy nanoparticles. *Science* **2018**, *359*, 1489–1494. [[CrossRef](#)] [[PubMed](#)]
13. Liu, M.; Zhang, Z.; Okejiri, F.; Yang, S.; Zhou, S.; Dai, S. Entropy-Maximized Synthesis of Multimetallic Nanoparticle Catalysts via a Ultrasonication-Assisted Wet Chemistry Method under Ambient Conditions. *Adv. Mater. Interfaces* **2019**, *6*, 1900015. [[CrossRef](#)]
14. Gao, S.; Hao, S.; Huang, Z.; Yuan, Y.; Han, S.; Lei, L.; Zhang, X.; Shahbazian-Yassar, R.; Lu, J. Synthesis of high-entropy alloy nanoparticles on supports by the fast moving bed pyrolysis. *Nat. Commun.* **2020**, *11*, 2016. [[CrossRef](#)] [[PubMed](#)]
15. Glasscott, M.W.; Pendergast, A.D.; Goines, S.; Bishop, A.R.; Hoang, A.T.; Renault, C.; Dick, J.E. Electrosynthesis of high-entropy metallic glass nanoparticles for designer, multi-functional electrocatalysis. *Nat. Commun.* **2019**, *10*, 2650. [[CrossRef](#)] [[PubMed](#)]
16. Simić, L.; Stopic, S.; Friedrich, B.; Zadavec, M.; Jelen, Ž.; Bobovnik, R.; Anžel, I.; Rudolf, R. Synthesis of Complex Concentrated Nanoparticles by Ultrasonic Spray Pyrolysis and Lyophilisation. *Metals* **2022**, *12*, 1802. [[CrossRef](#)]
17. Majerič, P.; Rudolf, R. Advances in Ultrasonic Spray Pyrolysis Processing of Noble Metal Nanoparticles. *Materials* **2020**, *13*, 3485. [[CrossRef](#)] [[PubMed](#)]
18. Toparli, C.; Ebin, B.; Gürmen, S. Synthesis, structural and magnetic characterization of soft magnetic nanocrystalline ternary FeNiCo particles. *J. Magn. Magn. Mater.* **2017**, *423*, 133–139. [[CrossRef](#)]
19. Jokanović, V.; Spasić, A.M.; Uskoković, D. Designing of nanostructured hollow TiO<sub>2</sub> spheres obtained by ultrasonic spray pyrolysis. *J. Colloid Interface Sci.* **2004**, *278*, 342–352. [[CrossRef](#)] [[PubMed](#)]
20. Ebin, B.; Gürmen, S. Synthesis and Characterization of Nickel Particles by Hydrogen Reduction Assisted Ultrasonic Spray Pyrolysis (USP-HR) Method. *KONA Powder Part. J.* **2011**, *29*, 134–140. [[CrossRef](#)]
21. Toparli, C.; Ebin, B.; Gürmen, S. Iron-Nickel-Cobalt (Fe-Ni-Co) Alloy Particles Prepared by Ultrasonic Spray Pyrolysis and Hydrogen Reduction (USP-HR) Method. In *Processing and Properties of Advanced Ceramics and Composites V*; John Wiley & Sons, Ltd.: Hoboken, NJ, USA, 2013; pp. 247–254. [[CrossRef](#)]
22. Raabe, D.; Tasan, C.C.; Olivetti, E.A. Strategies for improving the sustainability of structural metals. *Nature* **2019**, *575*, 64–74. [[CrossRef](#)] [[PubMed](#)]
23. Ma, Y.; Filho, I.R.S.; Bai, Y.; Schenk, J.; Patisson, F.; Beck, A.; van Bokhoven, J.A.; Willinger, M.G.; Li, K.; Xie, D.; et al. Hierarchical nature of hydrogen-based direct reduction of iron oxides. *Scr. Mater.* **2022**, *213*, 114571. [[CrossRef](#)]
24. Yang, Y.; Song, B.; Ke, X.; Xu, F.; Bozhilov, K.N.; Hu, L.; Shahbazian-Yassar, R.; Zachariah, M.R. Aerosol Synthesis of High Entropy Alloy Nanoparticles. *Langmuir* **2020**, *36*, 1985–1992. [[CrossRef](#)]
25. Stopic, S.; Hounsinaou, A.H.; Stéphane, K.A.; Husovic, T.V.; Emil-Kaya, E.; Friedrich, B. Transformation of Iron (III) Nitrate from an Aerosol by Ultrasonic Spray Pyrolysis and Hydrogen Reduction. *Metals* **2023**, *13*, 1686. [[CrossRef](#)]
26. Pan, F.; Liu, B.X. Formation of a metastable cubic phase in an immiscible Fe-Ag system by ion mixing. *J. Phys. Condens. Matter* **1993**, *5*, L315. [[CrossRef](#)]
27. Ardekani, S.R.; Aghdam, A.S.R.; Nazari, M.; Bayat, A.; Yazdani, E.; Saievar-Iranizad, E. A comprehensive review on ultrasonic spray pyrolysis technique: Mechanism, main parameters and applications in condensed matter. *J. Anal. Appl. Pyrolysis* **2019**, *141*, 104631. [[CrossRef](#)]

**Disclaimer/Publisher's Note:** The statements, opinions and data contained in all publications are solely those of the individual author(s) and contributor(s) and not of MDPI and/or the editor(s). MDPI and/or the editor(s) disclaim responsibility for any injury to people or property resulting from any ideas, methods, instructions or products referred to in the content.